Deuteron-induced reactions on ^{89}Y and nuclear level density of ^{90}Zr

Y. Byun, A. P. D. Ramirez, S. M. Grimes, A. V. Voinov, C. R. Brune, and T. N. Massey

Phys. Rev. C **90**, 044303 — Published 3 October 2014

DOI: 10.1103/PhysRevC.90.044303

Study of Deuteron Induced Reactions on ^{89}Y and Nuclear Level Density of ^{90}Zr

Y. Byun,* A. P. D. Ramirez, S. M. Grimes, A. V. Voinov, C. R. Brune, and T. N. Massey
Department of Physics and Astronomy, Ohio University, Athens, Ohio 45701, USA

Experimental elastic scattering and double differential cross sections of ^{89}Y(d,n) and ^{89}Y(d,p) reactions have been measured with 5, 6 and 7.44 MeV deuteron beams. It was found that about 76% of the total reaction cross section is determined by compound mechanism and rest is due to direct and pre-equilibrium interactions. Cross sections measured at backward angles were compared with calculations based on the compound nuclear Hauser-Feshbach model. It was found that it is possible to reproduce the backward angle neutron cross sections by compound model but it fails to describe proton cross sections. A pronounced peak is observed in neutron differential cross section which might result from strongly populated states 0^+, 4^-, and 5^- of ^{90}Zr via direct stripping reactions. The level density of ^{90}Zr has been obtained from neutron cross sections measured at backward angles. It is best described with the constant temperature level density model versus the traditional Fermi-gas one.

PACS numbers: 21.10.Ma,24.60.Dr,25.70.Gh,21.10.Pc

I. INTRODUCTION

The level density is one of the most important quantities for describing the statistical properties of excited nuclei. The density of discrete levels close to the ground state and neutron resonance spacings at the neutron separation energy have been studied experimentally for most of the nuclei on or near the line of beta-satiability so those results are well known. However, the level densities between the ground state and the neutron binding energy are still uncertain since the spacing between levels decreases rapidly with the increasing excitation energy so that levels cannot be resolved experimentally.

A common way to determine the level density is to make the interpolation between discrete levels and neutron resonance spacings by using such semi-empirical level density functions as the Fermi gas [1] and the Gilbert-Cameron (GC) ones [2]. However, the interpolation procedure is still considered to be uncertain since besides assumptions related to specific interpolation functions, it involves other uncertainties such as ones related to spin and parity distributions. Therefore, more reliable theoretical analysis and experimental efforts are needed to address this problem.

Another experimental method to obtain the nuclear level density in the energy range between the ground state and the neutron separation energy is the measurements of particle evaporation spectra from compound nuclear reactions [3]. The level density is extracted from the spectra of outgoing particles. The method is based on the Wolfenstein [4] and Hauser-Feshbach (HF) models [5] which utilize the Bohr independence hypothesis [6]. The advantage of this method compared to interpolation procedure is that it is less sensitive to spin and parity distributions and the energy dependence of the extracted level density is explicitly determined by the shape of the experimental particle spectrum. The assumption of the specific level density model function used in interpolation method is no longer needed. However, possible uncertainties caused by contribution of non-compound processes still need to be addressed by careful choice of specific nuclear reactions and interaction energies. Therefore the study of the reaction mechanism is an inherent part of the level density experimental study in each specific case.

In this work, the level density of ^{90}Zr was studied from the (d,n) reaction on ^{89}Y. The motivation of the choice of the ^{90}Zr nucleus is to study the level density of heavier nuclei compared to those we studied in our early works [3]. In addition, ^{90}Zr is a closed-shell nucleus with 40 protons and 50 neutrons. Therefore, we expect to see the unique nuclear structure effects in the experimental results, e.g., for stable closed-shell nuclei, level densities are expected to be less compared to nearly open-shell nuclei at the same excitation energies.

The ^{89}Y(d,d) and ^{89}Y(d,xp) reactions were also measured in order to get more insights on the mechanism of the d+^{89}Y reaction at these energies. In Sec. II the experimental set-up and data analysis are discussed. For ^{89}Y(d,n) reaction, the measured cross sections for two deuteron beam energies, the angular distributions for eight different angles, and the experimental results for the level density of ^{90}Zr are presented in Sec. II B. The experimental cross section and angular distributions for ^{89}Y(d,d) and ^{89}Y(d,xp) reactions are described in Secs. II A and II C. Finally, main results are summarized in Sec. III.

II. EXPERIMENTAL SETUP AND DATA ANALYSIS

The ^{89}Y$(d,n)^{90}$Zr experiment was carried out in the Edwards Accelerator Laboratory with two different deuteron energies of 6 (5.91) and 7.44 (7.36) MeV from the tandem Van de Graaff accelerator. Here, the numerical values in parenthesis are the actual deuteron beam energies due to the energy loss when it reaches the center of the target. The natural yttrium foil with thickness of 0.005 mm ($\simeq$ 3.253 mg/cm^2) was utilized as a target. The natural composition of the target consists of about 99.9% of ^{89}Y. For the measurement of the angular distribution of outgoing neutrons, the beam swinger facility was utilized by rotating the direction of the incoming beam and the target with respect to detector. The neutrons were detected by using a NE213 liquid scintillation de-

*Electronic address: yb283708@ohio.edu

tector at eight different angles, 150°, 140°, 120°, 105°, 90°, 71°, 45°, and 20°. The detector was located inside the well-shielded 30 m tunnel area. The energy of the outgoing neutrons was determined by using the time-of-flight method with a pulsed beam. For the given value of the detector diameter of 11.25 cm and the distance between the target and detector 6.75 m, the corresponding solid angle is 2.18×10^{-4} sr. The efficiency calibration of the neutron detector was achieved with the ^{27}Al(d,n) reaction. Neutrons were measured at 120° with E_d = 7.44 MeV. The efficiency was determined by comparing the measured neutron spectrum to the standard spectrum from the same reaction measured with a fission chamber [7, 8]. The standard neutron spectrum indicates the expected number of counts for a 100% efficient detector. The detector efficiency has been obtained to be about 25% for neutron energies of 2 MeV and it decreases down to about 20% for 12 MeV neutrons. We also measured the background spectrum with an empty target. The contributions from oxygen and carbon contaminations were estimated from corresponding peaks in neutron spectra. The contributions from background, carbon and oxygen contaminations were subtracted.

For ^{89}Y(d,d) and ^{89}Y(d,xp) reactions, the cross sections have been measured with 6 MeV deuterons using the charged particle time of flight spectrometer of the Edwards Accelerator Lab. The spectrometer consisted of seven 2m flight path tubes with Si detectors mounted at ends. The tubes were setup at 37.5, 52.5, 67.5, 97.5, 127.5, 142.5, 157.5 angles. The particle identification was performed with measuring the flight time and the energy deposited in Si detectors. The alpha channel has not been analyzed because of poor statistics due to low incident beam energy and high coulomb barrier for outgoing alpha particles. Experimental cross sections and energy of outgoing particles have been converted to the center of mass system for comparison with calculations.

A. ^{89}Y(d,d) elastic scattering

The angular distribution of 5,6 and 7 MeV elastic scattering deuterons is presented in Fig. 1 along with optical model calculations using different sets of optical model potentials from the compilation of Ref.[10]. Among presented calculations the closest one is from potentials of Ref.[21] although the deviation of about 10% at backward angles is observed. This deviation could be compensated by reducing the volume radius and/or diffuseness by about 20%. Adjusting parameters brings the absorbtion cross section down to 332 mb from the original 396 mb obtained with the potential of Ref.[21]. Knowledge of absorbtion cross section is important when comparing experimental outgoing particle differential cross sections with calculations.

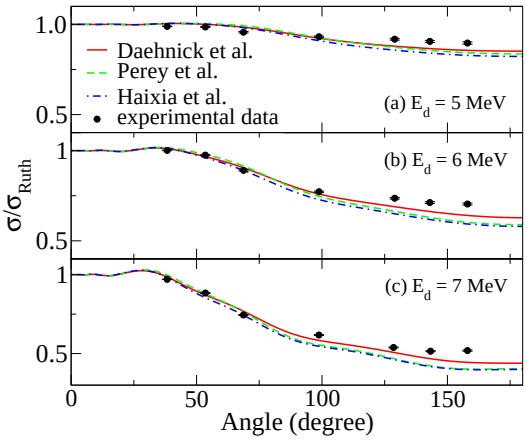

FIG. 1: (Color online) The angular distribution of elastically scattered deuterons on ^{89}Y. Points are experiment, lines are calculations with different optical model parameters according to Ref.[21] (Daehnick et al.), Ref.[22] (Perey et al.), Ref.[11] (Haixia et al.)

B. The ^{89}Y$(d,n)^{90}$Zr Reaction

1. *Angular distribution*

The analysis of the angular distribution of reaction products is an important tool to infer the reaction mechanism. Reactions can be divided on direct such as stripping and pickup, multistep direct (MSD), multistep compound (MSC) and compound ones. In case of MSC and compound reactions, the angular distribution of emitted particles is symmetric at about 90° [15] since the memory of the leading ejective is lost during the equilibration process. In Direct and MSD reactions, the outgoing particles tend to be emitted in the direction of the incident beam due to the fact that the equilibration process is not complete and the memory of the direction of an projectile is preserved. It is believed that outgoing particles which are due to compound nuclear mechanism dominate at backward angles. However, it is difficult to differentiate compound and MSC contributions because both of them have symmetric distribution at 90°.

Fig. 2 shows the experimental angular distributions of neutrons emitted from the ^{89}Y$(d,n)^{90}$Zr reaction measured with the deuteron beam energy of 7.44 MeV. Each point represents the cross section integrated over 2 MeV energy interval. It can be seen that the angular distribution is almost flat at backward angles where compound contribution dominates and there is an increase in cross sections at forwards angles due to the contribution of direct reaction. However, there is an exception for the energy range from 10 to 12 MeV where the pronounced peak is observed. The angular distribution in this energy range is a decreasing function even at backward angles. It means that there is a contribution to this peak from direct reactions even in backward angles. The same behavior should be valid for the corresponding peak for the 6 MeV of deuteron energy which is located between 8.5 and 10.5 MeV

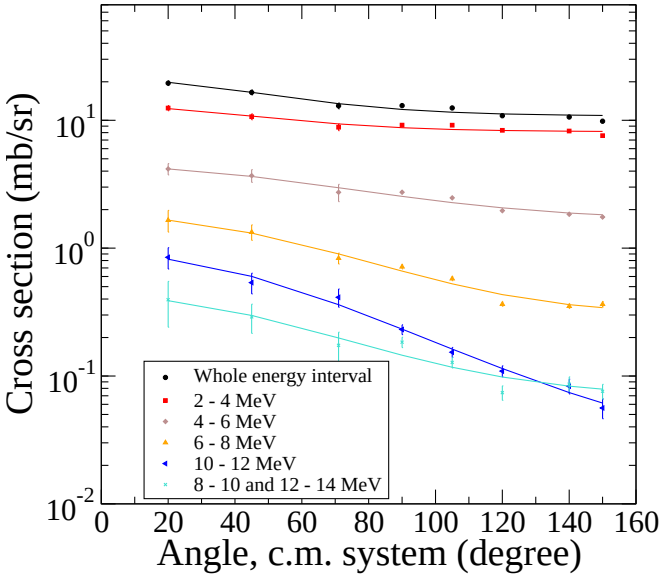

FIG. 2: (Color online) Angular distribution for different energy intervals of emitting neutrons from ^{89}Y$(d,n)^{90}$Zr reaction with 7.44 MeV deuteron beam. Solid lines represent the result of fitting (Eq. (1)) to experimental data points.

of neutron energies (see Fig. 3).

The angular distributions in Fig. 2 are fitted by using the following equation [15]

$$y = a_0 \exp(a_1 \cos\theta) + a2[\exp(a_3 \cos\theta) + \exp(-a_3 \cos\theta)], \quad (1)$$

where a_0, a_1, a_2, and a_3 are the fitting parameters. The first and second terms represent the contributions from direct and compound reactions, respectively. The parameter, a_3, representing the anisotropy of the angular distributions of the cross section in compound reaction, is set to zero for convenience since its value is supposed to be negligible. Eq. (1) has been shown [15] to reproduce a large variety of experimental angular distributions of nucleon and alpha induced reactions. According to our estimations based on Hauser-Feshbach model, the anisotropy caused by compound reactions such as (p,n) and (d,n) is expected to be less than 10%. The anisotropy is largely determined by orbital momentum of both incoming and outgoing particles. Therefore, higher momentum transfer reactions such as (α,n) would give us larger anisotropy which can be used for studying the parameter of the spin distribution (spin cutoff parameter) of residual nuclei. [16].

In order to determine the relative fractions of direct (forward peaked) and compound (isotropic) components, the angular distribution for the whole energy interval of neutrons has been fitted with the Eq. (1). To avoid excessive parameter correlations we assumed that three experimental points at most backward angles are entirely due to compound reaction mechanism. This assumption is supported by the fact that the experimental angular distribution at backward angles is flat. This is especially apparent for low energy neutrons which constitute the main fraction of the total (angle integrated) cross section. The flat angular distribution is consistent with the isotropic angular distribution expected from compound reactions. The high energy neutrons might contain some fraction of the pre-equilibrium non-isotropic component but the cross section of such neutrons is about two orders of magnitude smaller compared to that for low-energy neutrons (see Fig. 2). This allowed us to secure the parameter a_2 to be $10.4(\pm 0.3)$. The other fitting parameters were found to be $a_0 = 1.96(\pm 0.5), a_1 = 1.90(\pm 0.4)$. The resultant fraction of compound component is obtained to be (76±4%). This value is roughly in agreement with the estimation obtained for similar deuteron energies for ^{27}Al and ^{56}Fe targets [23].

2. $^{89}Y(d,n)$ *Cross section*

The experimental differential cross sections $(d\sigma/dE_n)(E_n)$ were determined in terms of the incoming deuteron beam current, the target thickness, and the detector efficiency. From the estimated systematic uncertainties for each component, the total uncertainty of the cross section is obtained to be about 25%. Fig. 3 shows the experimental cross sections measured at backward angles with deuteron energies of 7.44 and 6 MeV. Here, the experimental differential cross section are compared with theoretical calculations from the EMPIRE program [13]. Since backward angle cross sections are supposedly due to compound reaction mechanism, we used Hauser-Feshbach model for calculations.

The Hauser-Feshbach theory [4, 5] is based on the Bohr hypothesis and reciprocity theorem [9] to describe compound reaction cross reactions. According to this theory, the cross section of X(x,y)Y− reaction depends on transmission coefficients of outgoing particles y and on the level density of the residual nucleus Y. For the given total angular momentum, J, the partial cross section to final states of the residual nucleus is defined by

$$\sigma_{1,2}(J,S'_Y) = \frac{\pi}{k_1^2} \frac{(2J+1)}{(2s_x+1)(2S_X+1)} \frac{\sum_{l_1,j_1} \int dE_Y T_{l_1}(\varepsilon_1) \sum_{l_2,j_2} T_{l_2}(\varepsilon_2)\, \rho_Y(E^*_Y, S'_Y)}{\sum_{Y',l,j} \int dE_{Y'} T_{Y',l}\, \rho_{Y'}(E^*_{Y'})}, \quad (2)$$

where S'_Y is the angular momentum of final states in the residual nucleus Y, k is the wave number, and the term $(2J+1)/(2s_x+1)(2S_X+1)$ is the statistical factor, g_1, which is the probability to form a total angular momentum, J, by summing the relative angular momentum, l with the spin j. The range of the relative angular momentum, l, is from $|J-j|$ to $|J+j|$. Here the entrance channel spin, j_1, which is defined as the sum of the projectile spin s_x and target spin S_X, ranges from $|S_X - s_x|$ to $|S_X + s_x|$. Likewise, the exit channel spin, j_2, which is the sum of the residual nuclear spin, S_Y, and emitted particle spin, s_y, ranges from $|S_Y - s_y|$ to $|S_Y + s_y|$. T_{l_1}, T_{l_2}, and $\rho_Y(E^*_Y, S'_Y)$ are the incoming and outgoing transmission coefficients and the level density of the residual nucleus, Y, respectively. The term $\sum_{Y',l,j} T_{Y',l}\, \rho_{Y'}(E^*_{Y'})$ in the denominator

indicates the sum of all possible exit channels, which satisfy the conservation of angular momentum and energy. Here, ε_1 and ε_2 are the center-of-mass kinetic energy for the entrance (x + X) and exit (Y + y) channels represented by the number 1 and 2, respectively. These quantities in the formula are fixed for a given excitation energy of the compound nucleus, E_C^* and the final state of the residual nucleus, E_B^*, through the relation $\varepsilon_2 + E_B^* = E_C^* + Q_{c\to b+B}$ [9].

The transmission coefficients are calculated from the optical model potentials provided by the Reference Input Parameter Library (RIPL) database [10]. For the entrance channel, d+^{89}Y, we used potentials of Ref.[21] but with corrected volume radius and diffuseness to be able to reproduce elastic scattering of deuterons on ^{89}Y (see section II A). The optical potentials for the exit channel, ^{90}Zr+n, were deduced from the global systematics given by Koning and Delaroche [12]. Since the transmission coefficients are already well established, the cross section is strongly influenced by the nuclear level density.

The Empire program has several options for input level densities. These are Empire specific level density, the Ignatyuk model based on superfluid consideration [13], the Gilbert and Cameron model [2] and the microscopical model of Ref. [19]. Parameters of all the models (including microscopical one) are adjusted to reproduce experimental values of neutron resonance spacings. The calculations with GC and microscopical models are presented in Fig.3 versus experimental cross sections measured at backward angles. Ingnatyuk model has also been tested and found to be very close to GC one for this nucleus. Empire specific model largely overestimates experimental cross sections. Therefore calculations with these two models are not shown in Figure. Since the fusion cross section in calculations is assumed to be 100% compound but the neutron angular distribution in Fig. 2 indicates that 24% of the neutron cross section is due to non-compound contributions, the calculated double differential cross section for outgoing particles have been multiplied by the factor of 0.76. This factor takes into account the effective reduction of the deuteron flux which is responsible for the compound nucleus formation. This fraction has been estimated based on the neutron outgoing channel only. It was not possible to make the same estimation for the proton channel since the number of measured angles was restricted to backward angles only. Therefore we assume the same 0.76 factor to be valid for the protons. The possible uncertainties of this number do not affect the main conclusions of this paper because this is just the same scaling factor which is applied to the calculated cross sections of all outgoing channels. The sharp peaks observed above $E_n = 8.5$ and 6.5 MeV for E_d =7.44 and 6 MeV, respectively, correspond to discrete level region where the individual discrete levels of the known energy, spin and parity are used in calculations. One can see that calculations with default Empire level density models do not reproduce experimental data points well.

In Fig. 3, the pronounced peak is found in the range $10-11.5$ MeV and $8.5-10$ MeV for E_d =7.44 and 6 MeV, respectively. This peak is supposedly due to direct mechanism of the nuclear reaction populating discrete low-lying levels of

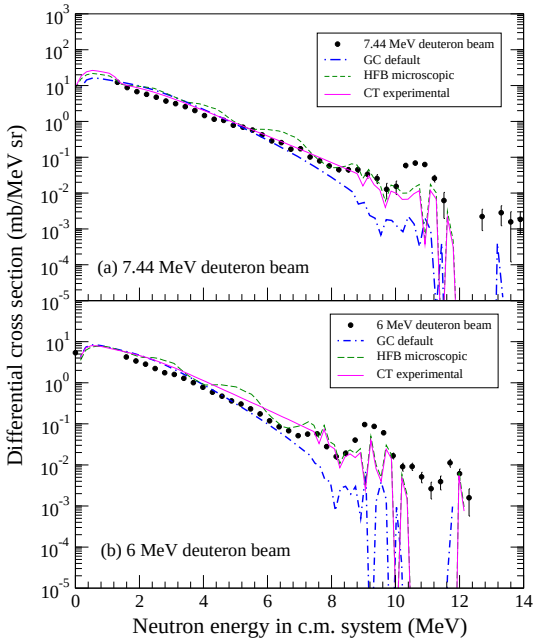

FIG. 3: (Color online) Experimental neutron evaporation spectrum (points) from the ^{89}Y$(d,n)^{90}$Zr reaction measured at backward angles with 7.44 and 6 MeV deuteron beam. Lines are EMPIRE calculations with different level density input models.

the ^{90}Zr nucleus. Table I displays discrete low-lying levels for ^{90}Zr in the energy range corresponding to peak locations in Fig. 3. As is described in Fig. 4, ^{89}Y absorbs a proton

TABLE I: Discrete levels for ^{90}Zr with excitation energies, E_x, and the corresponding emitted neutron energies in CM system, E_n, for different deuteron beam energies E_d.

Spin and parity	E_x (MeV)	E_n (MeV) E_d=7.44 MeV	E_n (MeV) E_d=6 MeV
0^+	0	13.1793	11.7740
0^+	1.7607	11.4381	10.0328
2^+	2.1863	11.0173	9.6119
5^-	2.3190	10.8860	9.4807
4^-	2.7393	10.4704	9.0650

producing the residual nucleus ^{90}Zr in the ^{89}Y$(d,n)^{90}$Zr reaction. The proton can occupy $2p_{1/2}$ state corresponding to 0^+ state of ^{90}Zr or may fill $1g_{9/2}$ state leading to 4^- or 5^- excited states. It means that the low-lying excited states of ^{90}Zr, 0^+, 4^- and 5^-, can be strongly populated via the direct stripping reaction. Since the decay into the excited states, 4^- and 5^-, produces the neutrons in the energy range where the peak is located, we can conclude that these two final states are strongly involved in the formation of the peak. Moreover, the cross sections in the region of the peak are greater than the theoretical calculations based on compound reaction

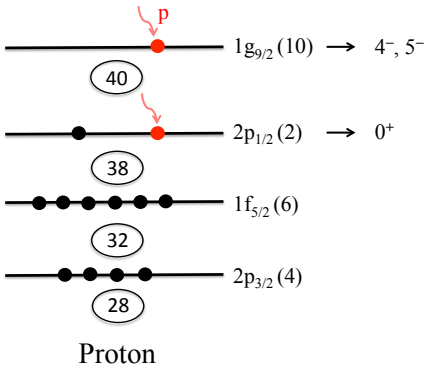

FIG. 4: (Color online) Proton single particle states of ^{89}Y (consists of 39 protons and 50 neutrons). In the ^{89}Y$(d,n)^{90}$Zr reaction, ^{89}Y absorbs a proton producing the residual nucleus ^{90}Zr. Proton can occupy $2p_{1/2}$ state corresponding to 0^+ state of ^{90}Zr or may fill $1g_{9/2}$ state leading to 4^- or 5^- excited states. The numerical values in parenthesis represent the occupation number for each state.

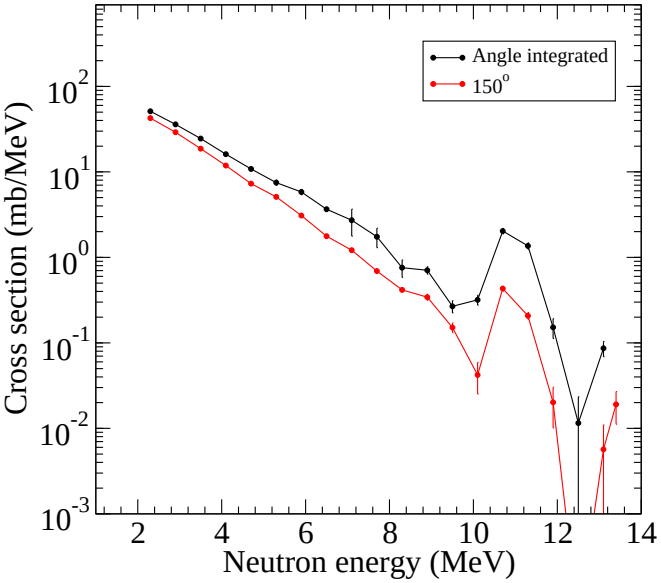

FIG. 5: (Color online) The angle-integrated neutron energy spectrum from ^{89}Y$(d,n)^{90}$Zr reaction with 7.44 MeV deuteron beam (see text). The double differential cross section measured at 150° and multiplied by 4π is also displayed for comparison.

model. Therefore, it might result from the contribution of direct reaction mechanism. In order to confirm that the proposed mechanism takes place, other type of reactions such as ^{87}Sr$(\alpha,n)^{90}$Zr need to be studied. This reaction is capable to eliminate one proton transfer mechanism and is expected to be more compound.

The angle-integrated neutron energy spectrum from ^{89}Y$(d,n)^{90}$Zr reaction with 7.44 MeV deuteron beam is shown in Fig. 5. In order to obtain this spectrum, the angular distributions for each 600 keV energy bin were fitted with Eq. (1) and the resulting fitting parameters were used to calculate the angle-integrated cross section over the solid angles. Compared to the cross section measured at 150 ° angle , the angle integrated neutron cross section is larger for higher neutron energies. Such behavior is expected because of the contribution from pre-equilibrium mechanism for higher energy neutrons.

3. *Level density of ^{90}Zr*

Since the level density is considered to be main uncertainty in compound reaction cross section calculations, the experimental level density of the residual nucleus can be deduced in terms of the measured and calculated differential cross sections in the following way [14]:

$$\rho(E) = \rho(E)_{input} \frac{(d\sigma/d\varepsilon)_{meas}}{(d\sigma/d\varepsilon)_{calc}}, \qquad (3)$$

where E is the excitation energy of the residual nucleus. Here, $(d\sigma/d\varepsilon)_{calc}$ and $(d\sigma/d\varepsilon)_{meas}$ are the calculated and experimental cross sections, respectively. The $\rho(E)_{input}$ is model input level density used in the calculations. Eq. (3) is based on Eq. (2) assuming that the transmission coefficients in Eq. (2) are fixed and the cross section is directly proportional to the level density of residual nucleus for the specific outgoing channel. The main uncertainties related to such an approach are connected to the validity of using the Eq. (2) for specific reactions. The EMPIRE program [13] was used to calculate cross sections in the framework of the Hauser-Feshbach theory. For the input level density, ρ_{input}, the Gilbert-Cameron model [2] was utilized. Parameters of the model were adjusted to reproduce the experimental data points as close as possible. The experimental nuclear level density is extracted then by using Eq. (3). The possible contribution from the second step neutron emission due to the (d,2n) reaction is not a concern since the energies of those neutrons are below the detection threshold.

Fig. 6 shows the experimental level density of ^{90}Zr extracted from the neutron cross section measured with 6 MeV of deuteron energy. The absolute normalization of the experimental level density has been performed by matching experimental data points to the density of discrete levels in the $\sim 3.5-5$ MeV energy interval. It can be seen that the experimental level density reproduces the shape of the known discrete levels in the low excitation energy range up to $E_x = 5$ MeV and then it starts to diverge. This divergence is due to the fact that discrete level scheme is not complete at higher excitation energies. The prominent step-like structure is observed at around 4 MeV and it can be tentatively explained by the breaking of Cooper pairs [20].

The data were fitted by using the Fermi-gas and the constant temperature models, which are defined by

$$\rho_F(E) \simeq \frac{\sqrt{\pi}}{12} \frac{\exp(2\sqrt{a(E-\delta)})}{a^{1/4}(E-\delta)^{5/4}} \frac{1}{\sqrt{2\pi}\sigma}, \qquad (4)$$

and

$$\rho_{CT}(E) = \frac{1}{T} e^{(E-E_0)/T}, \quad (5)$$

respectively. Here, a, δ, E_0, and T are adjustable parameters to fit experimental data. In the constant temperature model, the nuclear temperature, T, is assumed to be constant over the entire energy region indicating the possible phase transition which is supposed to occur when nucleus gains energy but the temperature remains constant. The spin-cutoff parameter, σ, characterizes the width of the distribution of the z-component of the nuclear angular momentum. We used the σ^2 suggested by von Egidy and Bucurescu [17] in the following form

$$\sigma^2 = 0.391 A^{0.675} (E - 0.5 P_d)^{0.312}, \quad (6)$$

where P_d is defined in [17] and related to the deuteron pairing energy and A is the mass number. The fits with the Fermi-gas and the constant temperature models are also shown in Fig. 6. Chi-square values and fitting parameters from both models along with parameters from von Egidy and Bucurescu systematics [17] are listed in Table II. It can be seen that the constant temperature fit shows better agreement with our experimental data points in the whole excitation energy interval from 4 to 10 MeV compared to the fit with the Fermi gas model.

TABLE II: Fitting parameters of level density models along with the predictions of von Egidy and Bucurescu systematics [17]. The deuteron pairing energy , P_d, used to determine the level density parameters for ^{90}Zr in this systematics is also shown.

Fermi gas model	a (MeV^{-1})	δ (MeV)	χ^2
Exp. fit	8.98(10)	2.58(8)	25.55
Theo. prediction (Von Egidy)	8.79(31)	1.32(20)	
Constant temperature model	E_0 (MeV)	T (MeV)	χ^2
Exp. fit	1.32(6)	0.99(1)	10.537
Theo. prediction (Von Egidy)	0.69(30)	0.91(4)	
deuteron pairing P_d (MeV)	3.394		

The level density is compared to the density of known discrete nuclear levels and to theoretical predictions of the Fermi-gas and the constant temperature models based on von Egidy and Bucurescu parameter systematics [17]. The level densities calculated with parameter systematics show considerable offset compared to experimental data points. The reason for the discrepancy is because the global parameter systematics of Ref. [17] do not always reproduce local experimental data. In our particular case of ^{90}Zr, the systematics reproduce well such parameters as a and T determining the general slope of the level density function. However, the systematics fail to reproduce the parameters, E_0 and δ, resulting in offset of predicted level density functions compared to experimental data points. Expected reduction of the level density for closed-shell nuclei is not taken into account properly for ^{90}Zr by the global systematics of Ref. [17].

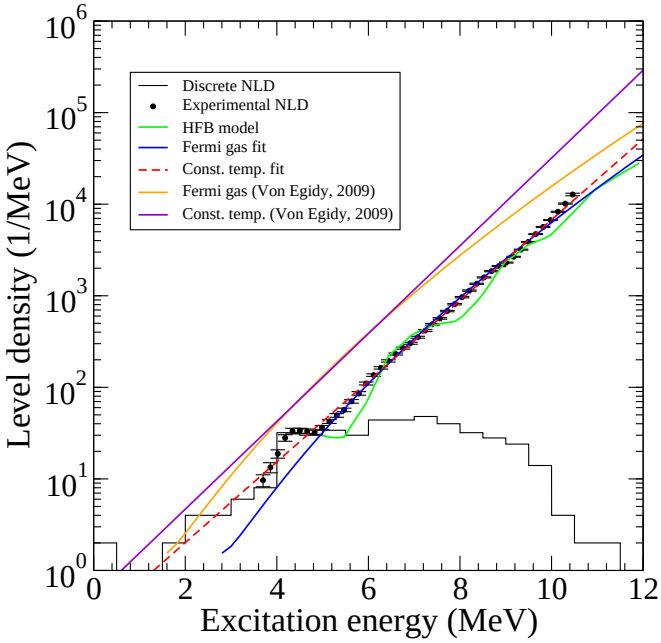

FIG. 6: (Color online) Comparison of the experimental level density of ^{90}Zr (full circle) with the density of known discrete levels from Ref. [18]. The fit of the Fermi-gas and the constant temperature models and the theoretical predictions for both models from Ref. [17] are shown. The level density obtained with the microscopic HFB model [19] is also displayed.

In addition, in Fig. 6, the experimental level density is also compared with the microscopic nuclear level density model used for (d,n) in Fig.3. This model is based on the Hartree-Fock-Bogoliubov (HFB) plus combinatorial method [19]. The HFB single-particle level scheme is taken into account along with collective rotational motion for deformed nuclei. The vibrational enhancement factor is newly introduced by considering the phonon excitations in order to describe extra low-energy phonon states, which cannot be explained with preexisting models. The vibrational enhancement results in oscillating energy dependence which is not supported by our experimental data points, although both the absolute magnitude and the general trend match data points well.

C. ^{89}Y(d,p) reactions

For E_d =6 MeV, the proton differential cross section measured at 127.5° and angular distributions are presented in Figs. 7 and 8, respectively. Unfortunately, because of the poor quality of the particle separation at forward angles, we only present the angular distribution for backward angles from 90^0 and up. The first calculation has been performed with Empire computer code [13] with level density model according to the Gilbert and Cameron prescription using default parameters of the Empire code. For the second calculation, the CT model for ^{90}Zr have been used with parameters found from the neutron spectrum in our experiment (see Table II). The final calculation has been performed with HFB microscopical model of

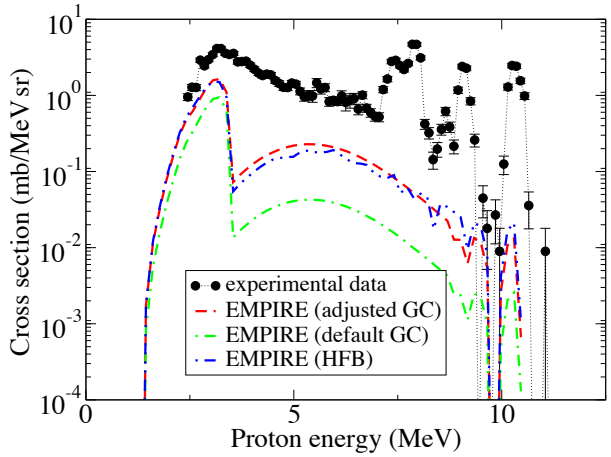

FIG. 7: (Color online) Differential cross section of ^{89}Y(d,xp). Points are experimental cross sections averaged over backward angle measurements, lines are calculations with different input level density models.

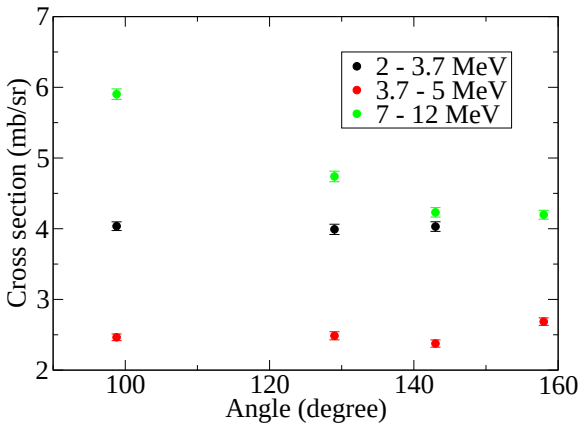

FIG. 8: (Color online). Angular distribution of protons from ^{89}Y(d,xp). Points are experimental cross sections integrated over indicated energy intervals.

Ref.[19] for all nuclei populated.

Even though the neutron differential cross section is well described by compound model calculations (except the pronounced peak discussed above, see Fig. 3), there is a sharp disagreement between compound reaction calculations and experimental data points for protons. Compound calculations strongly underestimate experimental cross section of the first generation protons which dominate in the energy region above around 3 MeV. Below this energy, there is a pronounced peak in calculations due to protons from (d,np) channel. There is no such a peak in the experimental spectrum. It is obvious that the experimental ratio of (d,p) and (d,np) cross sections is not reproduced by calculations based on compound mechanism of nuclear reactions

The angular distribution of protons is shown in Fig.8. Protons with energies 7-12 MeV populating discrete low lying levels exhibit forward peaked angular distribution indicating the dominance of the direct reaction mechanism. The angular distribution for lower energy protons is flat at backward angles indicating the dominance of compound reaction mechanism. It is surprising that even though protons from both (d,np) and (d,p) stages show similar angular distributions, the differential spectrum cannot be reproduced with calculations based on compound mechanism of nuclear reactions (see Fig.7). Both shape and absolute calculated cross sections are not consistent with experiment. Adjustment of level density parameters does not help as well. Such behavior for protons is not consistent with the neutron differential cross section in Fig.3 which is well described by compound reaction model. The possible explanation would have to be figured from considering other reaction mechanisms such as multistep-compound one which is also characterized by symmetric angular distribution at 90^0. One can also consider the second stage protons from (d,np), $(d,2p)$ or $(d,\alpha p)$ reactions where the first step is noncompound while the second step is compound. However, such numerical calculations with deuteron induced reactions are beyond our current capabilities. We would just like to point out the problem which might contain interesting physics.

III. SUMMARY AND CONCLUSIONS

The deuteron induced reaction on ^{89}Y was studied at the Edwards Accelerator Laboratory with the deuteron energies of 5, 6 and 7.44 MeV. The outgoing neutrons were detected at 8 different angles. The angular distribution was found to exhibit the forward peaked behavior. It can be explained by the direct reaction contribution to the total neutron cross section. For 7.44 MeV deuterons, the relative fraction of the compound component was found to be $76(\pm4)\%$. A study of deuteron induced reactions on ^{27}Al and ^{56}Fe has derived similar results for bombarding energies of 5 and 7 MeV [23].

The cross sections measured at backward angles were compared to Hauser-Feshbach model calculations using the EMPIRE reaction code. None of default level density models of Empire code were able to reproduce experimental data points. The validity of using the Hauser-Feshbach theory to analyze the neutron spectra is based on the assumption that the cross section measured at backward angles is entirely due to compound reaction mechanism. This is supported by the behavior of the neutron angular distribution at backward angles and partly by the fact that the Hauser-Feshbach calculations with some input level density functions (see Fig. 3 for HFB microscopic calculations) generally reproduce backward experimental cross section well. However, the validity of using the Hauser-Feshbach theory for this specific reaction cannot be proved by a single experiment. Experiments with projectiles other than deuterons are needed. The analysis of the experiments with He-3 and deuteron beams exciting the same compound nucleus has been done by us in Ref. [24] for the mass range around 55. The analysis showed that all outgoing neu-

trons and low-energy protons measured at backward angles are entirely due to compound reaction mechanism (they do not depend on type of projectiles).

The level density of ^{90}Zr has been extracted from neutron spectra measured at backward angles assuming the dominant contribution of compound reaction mechanism. The experimental level density was found to disagree with recent global level density systematics of Ref. [17] based on neutron resonance parameters. The systematics reproduce the slope of the nuclear level density but it shows a difference in magnitudes by a factor of 3. The level density calculated from HFB model follows an overall shape of experimental level density, however the presence of energy-dependent fluctions in HFB model are not supported by our experimental data.

Experimental level density points have been fitted by both the constant temperature and Fermi-gas models. The obtained chi-square values show the preference of the constant temperature model to reproduce the experimental data points. It indicates that the temperature does not depend on excitation energy of ^{90}Zr for the excitation energies up to about 11 MeV. From the extracted level density, we identified the step structure located at about 4-5 MeV of excitation energy. It presumably results from the breaking of Cooper pairs.

For the ^{89}Y$(d,n)^{90}$Zr reaction, a pronounced peak is found in the measured cross section corresponding to population of final levels in the $E_x = 1.5 - 3$ MeV excitation energy region of ^{90}Zr. The presence of this peak might result from the strongly populated low excited states, E_x = 1.76, 2.32, and 2.74 MeV with $J^\pi = 0^+$, 4^-, and 5^-, respectively, via the direct reaction. This phenomenon is directly related with the nuclear structure of ^{90}Zr, having the closed-shell with 40 protons and 50 neutrons. To study the origin of the observed peak, we need to perform additional measurements with a different reaction such as ^{87}Sr$(\alpha,n)^{90}$Zr one producing the same residual nucleus ^{90}Zr. Since more particle transfers are involved in this reaction, it would lead to the more complicated configuration, thus, the less pronounced peaks due to direct reactions are expected. In addition, the level density parameter, a, and the spin cutoff parameter σ can be deduced from the experimental emission spectra and angular distribution of ^{87}Sr$(\alpha,n)^{90}$Zr reaction.

The experimental cross sections for ^{89}Y(d,d) and (d,xp) reactions are also obtained. The angular distributions for both (d,np) and (d,p) outgoing channels show similar trend indicating the dominance of the compound mechanism of nuclear reaction. However, calculations based on compound reaction model fail to reproduce the experimental proton differential cross section. The reason might be due to the contribution of multistep-compound reaction but more investigations are required to resolve the discrepancy.

IV. ACKNOWLEDGMENTS

This work was performed with help of financial support of U.S. Department of Energy, Grant Numbers DE-FG02-88ER40387 and DE-NA0001837.

[1] H. A. Bethe, Phys. Rev. **50**, 332 (1936).
[2] A. Gilbert and A. G. W. Cameron, Can. J. Phys. **43**, 1446 (1965).
[3] A. V. Voinov, S. M. Grimes, U. Agvaanluvsan, E. Algin, T. Belgya, C. R. Brune, M. Guttormsen, M. J. Hornish, T. Massey, G. E. Mitchell, J. Rekstad, A. Schiller, and S.Siem, Phys. Rev. C **74**, 014314 (2006).
[4] L. Wolfenstein, Phys. Rev. **82**, 690 (1951).
[5] W. Hauser and H. Feshbach, Phys. Rev. **87**, 366 (1952).
[6] N. Bohr, Nature **137**, 344 (1936).
[7] T. N. Massey, S. Al-Quraishi, C. E. Brient, J. F. Guillemette, S. M. Grimes, D. Jacobs, J. E. O'Donnell, J. Oldendick and R. Wheeler, Nuclear Science and Engineering **129**, 175 (1998).
[8] W. B. Howard and S. M. Grimes and T. N. Massey and S. I. Al-Quraishi and D. K. Jacobs and C. E. Brient and J. C. Yanch, Nucl. Sci. Eng., **138**, 145(2001).
[9] A. J. Cole, *Statistical models for nuclear decay - From Evaporation to Vaporization*, (Institute of Physics Publishing, Bristol and Philadelphia, 2000).
[10] RIPL-1: Handbook for calculations of nuclear reaction data, IAEA, Vienna, Report No. IAEA-TECDOC-1024 (1998); RIPL-2: Handbook for calculations of nuclear reaction data, IAEA, Vienna, Report No. IAEA-TECDOC-1506 (2006); See also http://www-nds.iaea.org/RIPL-2/
[11] Haixia An and Chonghai Cai, Phys. Rev. C **73**, 054605 (2006).
[12] A. J. Koning and J. P. Delaroche, Nucl. Phys. A **713**, 231 (2003).
[13] M. Herman, R. Capote, P. Oblozinski, and A. Trkov, http://www. nndc.bnl.gov/nndcscr/model-codes/empire-ii/
[14] A. Wallner, B. Strohmaier, and H. Vonach, Phys. Rev. C **51**, 614 (1995).
[15] C. Kalbach, Phys. Rev. C **37**, 2340 (1988).
[16] S. M. Grimes, J. D. Anderson, J. W. McClure, B. A. Pohl, and C. Wong, Phys. Rev. C **10**, 2373 (1974).
[17] T. von Egidy and D. Bucurescu, Phys. Rev. C **80**, 054310 (2009).
[18] Data extracted using the NNDC On-Line Data Service from the ENSDF database, Available online at http://www.nndc.bnl.gov/chart/
[19] S. Goriely, S. Hilaire, and A. J. Koning, Phys. Rev. C **78**, 064307 (2008).
[20] A. Schiller, E. Algin, L. A. Bernstein, P. E. Garrett, M. Guttormsen, M. Hjorth-Jensen, C. W. Johnson, G. E. Mitchell, J. Rekstad, S. Siem, A. Voinov, and W. Younes, Phys. Rev. C **68**, 054326 (2003).
[21] W. W. Daehnick, J. D. Childs and Z. Vrceli, Phys. Rev. C **21**, 2253 (1980).
[22] C. M. Perey and F. G. Perey, Atomic Data and Nuclear Data Tables **13**, 293 (1974).
[23] S I. Al-Quraishi, C. E. Brient, S. M. Grimes, T. N. Massey, J. Oldendick and R.Wheeler, Phys. Rev. C **62**, 044616 (2000).
[24] A. V. Voinov, S. M. Grimes, C. R. Brune, M. J. Hornish, T. N. Massey and A. Salas, Phys. Rev., C76, 044602 (2007).